Room Temperature Ionic Liquid−Lithium Salt Mixtures: Optical Kerr Effect Dynamical Measurements

Bruno G. Nicolau,[†] Adam Sturlaugson,[‡] Kendall Fruchey, Mauro C. C. Ribeiro,[†] and M. D. Fayer*[,‡]

Laboratório de Espectroscopia Molecular, Instituto de Química, Universidade de São Paulo, C.P. 26077, CEP 05513-970, São Paulo, SP, Brazil, Department of Chemistry, Stanford University, Stanford, California 94305

Received: April 27, 2010; Revised Manuscript Received: May 22, 2010

The addition of lithium salts to ionic liquids causes an increase in viscosity and a decrease in ionic mobility that hinders their possible application as an alternative solvent in lithium ion batteries. Optically heterodyne-detected optical Kerr effect spectroscopy was used to study the change in dynamics, principally orientational relaxation, caused by the addition of lithium bis(trifluoromethylsulfonyl)imide to the ionic liquid 1-butyl-3-methylimidazolium bis(trifluoromethylsulfonyl)imide. Over the time scales studied (1 ps−16 ns) for the pure ionic liquid, two temperature-independent power laws were observed: the intermediate power law (1 ps to ∼1 ns), followed by the von Schweidler power law. The von Schweidler power law is followed by the final complete exponential relaxation, which is highly sensitive to temperature. The lithium salt concentration, however, was found to affect both power laws, and a discontinuity could be found in the trend observed for the intermediate power law when the concentration (mole fraction) of lithium salt is close to $\chi(LiTf_2N) = 0.2$. A mode coupling theory (MCT) schematic model was also used to fit the data for both the pure ionic liquid and the different salt concentration mixtures. It was found that dynamics in both types of liquids are described very well by MCT.

I. Introduction

Room temperature ionic liquids (RTILs) have been the object of extensive study in the past decade due to their unique properties, including very low vapor pressure and nonflammability under ambient conditions, selective reaction medium, etc.[1−4] One particular area of interest is the possible use of ionic liquids as alternative solvents in lithium ion batteries. The current generation of such batteries uses organic compounds as solvents.[5,6] These solvents present safety issues due to their volatility and high flammability. Thus, RTILs could become a greener and safer alternative.

Several studies reported that the addition of inorganic lithium salts to RTILs leads to an increase in viscosity and deleterious effects on relevant electrochemical properties, such as the ionic mobility of the lithium ion.[7−11] The cause of this effect has been extensively studied by Raman spectroscopy. The vibrational mode of the bis (trifluoromethylsulfonyl)imide ($[Tf_2N]^-$) anion found at $\nu \sim 740$ cm^{-1} displays a concentration-dependent shift to $\nu \sim 747$ cm^{-1} with the introduction of Li^+ in the ionic liquid system. This shift has been interpreted in terms of ionic pairing with the addition of a highly polarizing ion such as lithium.[12−17] Molecular dynamics simulations[13,18] show that the introduction of cations such as Li^+ into the mixture causes aggregation of the $[Tf_2N]^-$ anion around the small cations, resulting in higher viscosities and reducing their mobility. This is similar in a number of ways to the effect (known as the Chemla effect) observed in molten inorganic salt mixtures such as LiF/KF,[19] in which the introduction of the lithium ion leads to a system with lower ionic mobility than both of the pure substances.

In this work, optically heterodyne-detected optical Kerr effect (OHD-OKE) spectroscopy, which measures the time derivative of the polarizability−polarizability correlation function (second Legendre polynomial correlation function), is used to probe the orientational dynamics of pure 1-butyl-3-methylimidazolium bis(trifluoromethylsulfonyl)imide ([bmIm][Tf_2N]) over a wide range of temperatures and concentrations of lithium bis(trifluoromethylsulfonyl)imide ($LiTf_2N$). OHD-OKE experiments provide important insights into the nature of the ionic pairing by analyzing the dynamics over a wide range of times and observing the effects of "caging" in the systems.

The OHD-OKE technique has been extensively used for studies of liquid crystals;[20−23] molecular liquids;[24−31] and, to some extent, ionic liquids[32−36] over time spans from subpicosecond to tens of nanoseconds and longer. The studies of supercooled liquids were carried out over a wide range of temperatures, ranging from room temperature to temperatures lower than the mode coupling transition temperature, T_c. It has been found that, for all data, the time derivative of the polarizability−polarizability correlation function, $F(t)$, can be described by a decay composed of several power laws with the longest time scale, corresponding to complete orientational relaxation, being exponential. Although full schematic mode coupling theory (MCT) was used to analyze data, it was found that the following phenomenological MCT-based equation, which has been used previously,[21,23−26,32,33] gives a simple and accurate model of the data.

$$F(t) = [at^{-s} + pt^{-z} + dt^{b-1}]e^{-t/\tau_\alpha} \quad (1)$$

The first power law, at^{-s}, describes the subpicosecond relaxation dynamics referred to as the fast β processes; followed by a crossover region, where the "intermediate power law", pt^{-z},

* Corresponding author. E-mail: fayer@stanford.edu.
[†] Universidade de São Paulo.
[‡] Stanford University.

10.1021/jp103810r
Published on Web 06/09/2010

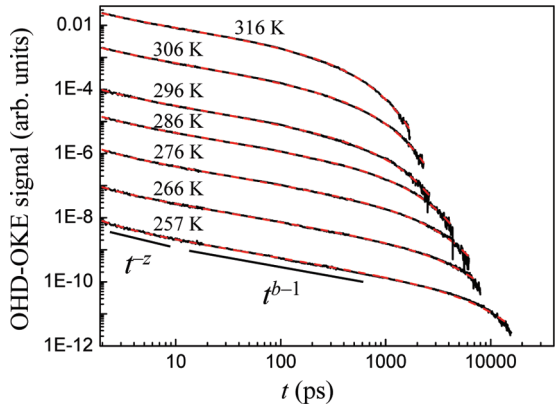

Figure 1. OHD-OKE data for [bmIm][NTf_2] at several temperatures (black curves). The curves are offset vertically to facilitate viewing. The results of fitting the data are the dashed red curves. The lines below the 257 K data are aids to show the two power laws that precede the final exponential decay.

is observed; and then the longest time scale von Schweidler power law, dt^{b-1}. The power laws are followed by a highly temperature- and concentration-dependent exponential decay, the α relaxation, which results in the final complete randomization of the molecular orientations. The intermediate and von Schweidler power laws are indicated in Figure 1, which will be discussed in detail below.

Along with the phenomenological fitting function given above, the Sjögren MCT schematic model was used to fit all data to obtain a set of parameters that was used to compare the systems studied. The schematic model uses an orientational correlation function coupled to a density correlation function,[37] which has been very successful in describing the dynamics in other liquid systems.[22,33,38] The model yields the time-dependent shapes of the data as well as temperature-dependent scaling functions, which can be used to test MCT's applicability to the systems studied.

II. Experimental Procedures

The OHD-OKE technique consists of an initial pump pulse responsible for generating an orientational anisotropy in the sample, which results in a birefringent medium. A time-delayed probe pulse heterodyne detects the relaxation of the pump induced birefringence. The signal decays over time due to orientational relaxation processes.[39] OHD-OKE spectroscopy observes the time derivative of the polarizability−polarizability correlation function (second Legendre polynomial correlation function), which at all but the shortest times is related to the molecular orientational relaxation. At very short times, there are additional contributions from interaction or collective collision induced dynamics. There can also be oscillatory components to the signal at very short times, less than a few picoseconds, which arise from intramolecular and intermolecular vibrational modes. The signal depends on the polarizability anisotropy and the magnitude of the polarizability. In these experiments, the molecular cations and anions have similar contributions to the signal. The Fourier transform of the OHD-OKE signal is directly related to depolarized light scattering.[40−42]

A Ti:sapphire 5 kHz oscillator-regenerative amplifier was used to generate both pump and probe pulses. The regen compressor was used to control the duration of the pump pulse (from 50 fs to 125 ps). The increased pump duration produces better signals for the long-time portions of the data. A 70 fs pulse was used to take data up to 15 ps, and a 2.5 ps pulse was used for data up to 550 ps. These time ranges were scanned with a stepper motor delay line. The 125 ps pulse and a long delay line were used to observe dynamics up to 16 ns. These sets of data were taken so that they partially overlap in time and were merged, adjusting only their relative amplitudes.

The data reported here are the pure heterodyne signal with no homodyne contribution. The homodyne contribution is eliminated by phase cycling. The quarter wave plate in the probe beam that produces the local oscillator that heterodynes the signal is rotated between two positions on alternate scans of the delay line. The two positions change the sign of the heterodyne signal but do not affect the homodyne signal. The two scans are subtracted, which has the effect of adding the heterodyne signals and removing the homodyne signals. Many pairs of scans are averaged to produce the data used for analysis.

The ionic liquid [bmIm][Tf_2N] was purchased from Iolitec and heated to 65 °C on a sand bath under vacuum for 24 h to remove water residue. After this process, the water residue was measured by Karl Fischer titration and found to be 50 ppm. $LiTf_2N$ was purchased from Aldrich and used without further purification. Both were kept in a glovebox under nitrogen (water and oxygen content kept lower than 1 ppm). The samples were used after filtration through a 0.5−1.5 μm filter (depending on the viscosity) to remove dust particles and reduce scattered light.

Viscosity measurements were carried out utilizing a Texas Instruments AR-G2 rheometer. During the viscosity measurements, samples were kept in a nitrogen atmosphere to prevent the absorption of water.

III. Results and Discussion

A. Temperature Dependence of the Pure Liquid. Temperature-dependent experiments were carried out for pure [bmIm][Tf_2N] to determine if its dynamics are in accord with those observed for systems studied in the past.[20,21,24−26,32,33,43] Data, as displayed in Figure 1, were obtained for temperatures ranging from 316 to 257 K. For times shorter than 500 fs, the signal is dominated by the electronic response of the sample. In addition, the large bandwidth of the laser pulse results in stimulated Raman scattering excitation of intramolecular and intermolecular low frequency vibrational modes. The signal from these modes obscures the liquid's dynamics for times less than ∼2 ps and prevents the fast beta process (at^{-s}, the first term in eq 1) from being observed. Therefore, the data were fitted starting at ∼2 ps using eq 1 but omitting the first power law.

Data will also be discussed in terms of the schematic mode coupling theory. Ideal MCT describes the coupled local density fluctuations of a system. As discussed further below, the orientational relaxation correlation function (polarizability−polarizability correlation function) measured in the OHD-OKE experiment is coupled to the density correlation function with the result that the same features that appear in the density correlation function also manifest themselves in the orientational correlation function.[22,37] Thus, the dynamics embodied in the relaxation terms in the phenomenological eq 1 also are found in the solutions to the coupled density-orientation MCT equations.

Figure 2 displays the intermediate and von Schweidler exponents z and b respectively, as a function of temperature obtained from fits using eq 1 (dashed red curves) to the data (black curves) displayed in Figure 1. Within experimental error, both exponents are temperature-independent. The lines through the points in Figure 2 are the average values of the exponents. The temperature-independent values of z and b are 2.16 ± 0.09 and 0.44 ± 0.01, respectively. These values can be compared to previously reported "normal" values obtained from the study of a variety of liquids.

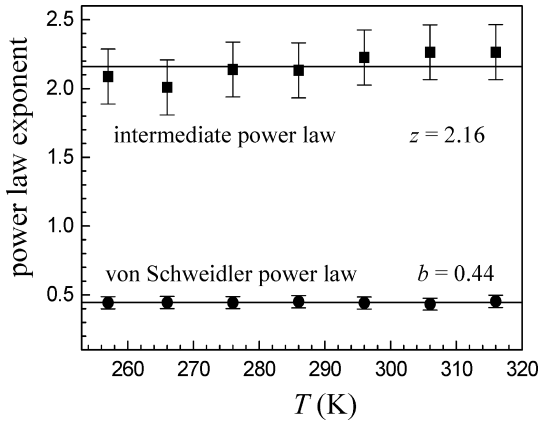

Figure 2. The exponents of the intermediate power law (z) and the von Schweidler power law (b) as a function of temperature. Both exponents are temperature-independent within experimental error.

The value observed for b falls close to the reported value of 0.49 measured for the RTIL 1-propyl-3-methylpyridinium bis(trifluoromethylsulfonyl)imide,[33] which was thought to be abnormal up to this point. Both values for RTILs are at the low end of the range of values observed for nonionic organic liquids, such as dibutylphthalate ($b = 0.57$).[25,44]

The range of values found for z in nonionic organic liquids, liquid crystals, and the RTIL 1-propyl-3-methylpyridinium bis(trifluoromethylsulfonyl)imide is 0.63−1.00.[20,21,24−26,32,33,43] with a value of $z = 1$ for the RTIL. Therefore, the value $z = 2.16$ found for [bmIm][Tf_2N] is very different from the many values measured previously on a variety of systems. As shown below, this is not caused by the inapplicability of MCT to [bmIm][Tf_2N]. The value found for z shows that the short time scale cage relaxation of this liquid is substantially faster than has been observed before. It is possible that this very large value of z might be found for other RTILs, but at this junction, the z value of [bmIm][Tf_2N] suggests that it has unusual short time dynamics.

The data fitting using eq 1 and the description of the terms assumes that MCT can be applied to describe the data. MCT supplies tools to analyze its applicability. MCT provides scaling relationships that can be used to determine the MCT critical temperature (T_c), which is the temperature in the theory at which the system becomes nonergodic.[45−47] T_c, which was initially thought to be the glass transition temperature, is typically 15−20% higher than T_g.[44]

The MCT scaling relations give the temperature dependence of the α relaxation exponential decay constant, τ_α, and the amplitude of the von Schweidler power law, d, (see eq 1) to the temperature-independent von Schweidler power law exponent, b (see Figure 2 and eq 1).

$$\tau_\alpha \propto (T - T_c)^{-\gamma} \tag{2}$$

with γ given by

$$\gamma = (a + b)/2ab \tag{3}$$

a is found from the von Schweidler power law exponent b using

$$\Gamma^2(1 - a)/\Gamma(1 - 2a) = \Gamma^2(1 + b)/\Gamma(1 + 2b) \tag{4}$$

where Γ is the gamma function.

$$d \propto (T - T_c)^{\delta} \tag{5}$$

where δ is given by

$$\delta = (a + b)/2a \tag{6}$$

Using $b = 0.44$ (see Figure 2), the values for γ and δ are 2.99 and 1.33, respectively. The scaling relations state that plots of $d^{1/\delta}$ and $\tau_\alpha{}^{-1/\gamma}$ vs T should give straight lines with intercepts of T_c. Figure 3 shows plots of the scaling relations. As can be seen, the data for both scaling relations fall on straight lines. The intercepts are 227 and 222 K, which give essentially the same value of T_c within experimental uncertainty. Therefore, T_c is ∼225 K.

The reported value for the [bmIm][Tf_2N] glass transition temperature is 187 K, resulting in $T_c/T_g = 1.2$, which falls within the range expected from experiments on many other liquids. The agreement of the data with the MCT scaling relations supports the applicability of MCT to describe the time-dependent data. It is remarkable that the temperature dependence of the exponential α relaxation time constant, τ_α, can be predicted simply by knowing the exponent of the von Schweidler power law.

The schematic MCT model describes the coupled wave vectors for the density fluctuations in a liquid in terms of a damped harmonic oscillator coupled to a memory function.[37,38,45] The memory function reflects the short time caging effect that gives rise to the power law decays and only at long times goes into the complete exponential structural relaxation. The initial MCT theory described only density fluctuations. To properly describe OHD-OKE data or dynamic light scattering data, both of which measure an orientational relaxation correlation function (polarizability−polarizability correlation function), it was necessary to extend the theory to include an orientational correlation function equation that is coupled to the density correlation function.[37,38] The orientational correlation function measured in these experiments has the same behavior as the density−density correlation function tracked by MCT. The result is a model consisting of two damped oscillators coupled to two memory functions.[37]

There are two correlation functions: $\phi_1(t)$, associated with density fluctuations, and $\phi_2(t)$, which is the observable correlation function (in the present case, the autocorrelation function of the polarizability anisotropy).

$$\ddot{\phi}_i(t) = -\Omega_i^2\,\phi_i(t) - \mu_i\,\dot{\phi}_i(t) - \Omega_i^2 \int_0^t \mathrm{d}\tau\, m_i(t - \tau)\,\dot{\phi}_i(\tau) \qquad i = 1, 2 \tag{7}$$

where $\Omega_{1,2}$ are the characteristic frequencies and $\mu_{1,2}$ are the damping constants. The memory functions have the following forms:

$$m_1(t) = \nu_1\,\phi_1(t) + \nu_2\,\phi_1{}^2(t) \tag{8}$$

and

$$m_2(t) = \kappa\,\phi_2(t)\,\phi_1(t) \tag{9}$$

$\nu_{1,2}$ are constants in the density memory function, and κ is the translational−rotational coupling constant. The second correlator

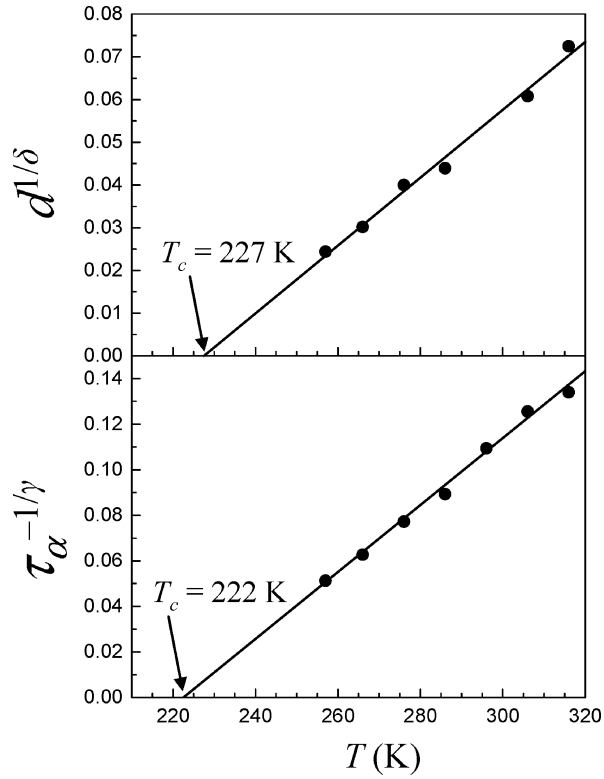

Figure 3. MCT scaling plots for the von Schweidler power law amplitude d (top panel) and the α relaxation time constant τ_α (bottom panel) obtained from the data and eqs 2−6. The lines presented are linear fits to the data. The points fall on the lines as predicted by the MCT scaling relations and have intercepts that are the MCT critical temperature, T_c. The two values of T_c are almost the same and give an average value of 225 K.

has short-time damped harmonic oscillator behavior governed by μ_2 and Ω_2, and its coupling to the density correlator via the parameter κ largely determines its longtime behavior.

The time- and temperature-dependent data shown in Figure 1 were fitted with the MCT described in eqs 7−9. The fits and the quality of the fits are essentially identical to those shown by the red dashed curves in Figure 1. The ability of the MCT theory to fit the data over a wide range of times and temperatures is consistent with MCT fits to other liquids: for example, acetylsalicylic acid, dibutylphthalate, *N*-propyl-3-methylpyridinium bis(trifluoromethylsulfonyl)imide, and 1-ethyl-3-methylimidazolium tosylate,[33,38] for which MCT was able to reproduce the experimental curves. The values of Ω_1 and Ω_2 were found not to affect the trends observed for the rest of the parameters. As a result, they were fixed at a $\Omega_1 = 0.5$ THz and $\Omega_2 = 1.0$ THz, in accord with the procedure adopted for molecular liquids and ionic liquids previously studied.[33,38] Temperature-independent behavior was observed for the damping constant of the density−density correlation function, μ_1. Its value was fixed at the center of the range of possible values. The choice of μ_1 changes the values of the remaining constants to some extent, but the trends observed are unaffected. The translational-rotational coupling constant κ is found to increase as temperature decreases.

The theoretical ergodic (liquid phase) to nonergodic (ideal glassy phase) transition, which occurs at T_c, can be described in terms of variation of the density−density coupling constants by constructing a phase diagram in which the variation of ν_1 is plotted against ν_2.[33,48] ν_1 and ν_2 are determined as a function of temperature from the fits to data like those shown in Figure 1.

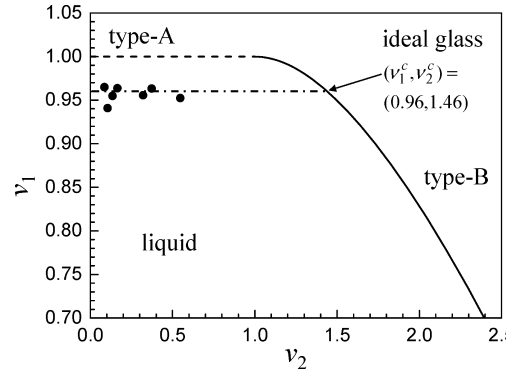

Figure 4. The MCT phase diagram representing the variation of parameters ν_1 and ν_2 with temperature. Type A and type B transitions, shown as the dashed and solid lines, respectively, represent the boundary between the liquid (ergodic) and the ideal glass (nonergodic). The horizontal line passing through the points determined by fitting the experimental data is the trajectory in the ν_1, ν_2 space. Where the trajectory crosses the liquid-ideal glass boundary yields the critical values, (ν_1^c, ν_2^c), which are virtually identical to the calculated values (see text).

A plot of (ν_1, ν_2) is a trajectory in the ν_1, ν_2 space. Where the trajectory crosses the boundary between the liquid (ergodic) and ideal glass (nonergodic) states gives the critical values, ν_1^c, ν_2^c. MCT predicts the theoretical values for these parameters, which occur at the liquid-to-ideal glass transition.

Figure 4 displays a ν_1^c, ν_2^c plot. The data were obtained only for temperatures well above T_c. As can be seen from the plot, ν_1 is temperature-independent within experimental error. The temperature dependence is in ν_2, the coefficient of the quadratic term in the memory function. The dot−dash line shows a linear fit extrapolated to the liquid−ideal glass boundary. As shown in the figure, (ν_1^c, ν_2^c) = (0.96, 1.46).

These critical parameters can be obtained from MCT using only the experimental value of the von Schweidler power law exponent, b.[33,48] Defining,

$$\lambda = \Gamma^2(1 + b)/\Gamma(1 + 2b) \tag{10}$$

then

$$\nu_1^c = (2\lambda - 1)/\lambda^2 \tag{11}$$

and

$$\nu_2^c = 1/\lambda^2 \tag{12}$$

Using the experimental value of $b = 0.44$, (ν_1^c, ν_2^c) = (0.95, 1.49). The experimental and calculated values of ν_1^c and ν_2^c are seen to be in excellent agreement. These results and the other results presented above show that the dynamical behavior of [bmIm][Tf_2N] is well described by MCT. These results give confidence that we can use parameters associated with MCT in analyzing the influence of lithium ions on [bmIm][Tf_2N].

B. The Influence of Lithium Ions. Experiments were conducted to investigate the changes in the dynamics of the ionic liquid with the introduction of the lithium cation. Samples were prepared with different concentrations of Li^+, ranging from $\chi(LiTf_2N) = 0$ to 0.40. For mole fractions above 0.40, it was not possible to obtain a homogeneous solution.

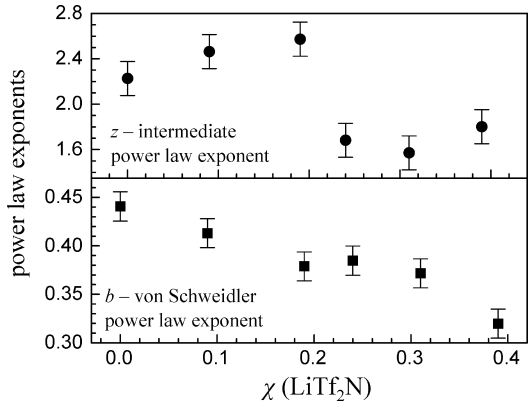

Figure 5. Lithium salt concentration-dependent behavior of the intermediate power law exponent z (top panel) and the von Schweidler power law exponent, b. The exponents are concentration-dependent, in contrast to Figure 2, where the exponents are temperature-independent. The value of b is found to decrease with the increase of $\chi(LiTf_2N)$. A discontinuity in the trend observed for z is found at $\chi(LiTf_2N) = 0.2$. b shows an inflection point around 0.2.

The intermediate power law exponent, z, and the von Schweidler exponent, b, (see eq 1 and Figure 2) were found to be temperature-independent for the pure liquid. This is in contrast to the behavior found as the concentration of lithium cation is varied. Figure 5 shows the substantial changes in the intermediate and von Schweidler power law exponents with lithium concentration. The von Schweidler exponent decreases as the concentration of Li^+ increases. There appears to be an inflection point at $\chi = 0.2$. Figure 2 shows that b can be determined with very little error in the values. Therefore, it is likely that the inflection point is real. The von Schweidler power law leads to the final complete structural relaxation, which is the exponential α relaxation. b reflects the final decay of the caging that precedes the complete structural relaxation. The results suggest that the addition of lithium cations slows this process.

The intermediate power law exponent displays an abrupt change at $\chi(LiTf_2N) = 0.2$. As the concentration of Li^+ is increased, first z increases significantly. At ~0.2, there is a sudden drop and then a small increase with further increase in concentration. This is at the same mole fraction at which the change in the von Schweidler power law shows an inflection point. Raman spectroscopy has been used to examine structural changes as a function of Li^+ concentration in this RTIL system.[14] A distinct change was observed at $\chi(LiTf_2N) = 0.19$. The observed change in the Raman spectrum was interpreted as a structural change, that is, a change in the lithium coordination number. Below 0.2, ionic structures of the form $Li(Tf_2N)_2$ occur, but above 0.2, they are more likely to be $Li(Tf_2N)_4$ or even $Li(Tf_2N)_5$. The Li^+ concentration dependence of both the intermediate power law and the von Schweidler power law show that dynamics of the RTIL are substantially influenced by the addition of lithium cation in a manner that is quite distinct from the dynamical changes associated with changing the temperature. The previous Raman studies indicate that these dynamical changes may be associated with structural changes in the liquid.

The final exponential decay (α relaxation) reflects the complete orientational randomization of the molecules. Frequently, orientational relaxation is described well by the Debye−Stokes−Einstein (DSE) equation. Identifying τ_α as the orientational relaxation time constant, then the DSE equation is

$$\tau_\alpha = \frac{V_{eff}\eta}{k_B T} \tag{13}$$

where k_B is Boltzmann's constant, T is the absolute temperature, η is the viscosity, and V_{eff} is the effective volume. The effective volume includes shape factors for the nonspherical particles and the boundary condition.[49−51] The orientational relaxation time constant is related to the orientational diffusion constant as $\tau = 1/6D_\theta$. Equation 13 shows that at fixed temperature, τ_α is linear in the viscosity. If this relationship is obeyed, the orientation relaxation is considered to be "hydrodynamic".

Table 1 gives τ_α, D_θ, and η for the $LiTf_2N$ mole fractions that were studied. The viscosities are in centipoise (cP). As can be seen from the table, τ_α increases substantially as the mole fraction, and therefore, the viscosity increases. To determine if the orientational relaxation is hydrodynamic, the products $D_\theta\eta$ are plotted as a function of $LiTf_2N$ mole fraction in Figure 6. If the system is hydrodynamic, that is, the diffusion constant is inversely proportional to the viscosity, the products should fall on a horizontal line. Using the pure liquid as the starting point, the hydrodynamic line is shown in Figure 6. As is clear from the figure, the complete diffusive orientational relaxation (α relaxation) is not hydrodynamic. The product first decreases with increasing $LiTf_2N$ mole fraction and then increases again. The initial drop below the line indicates that the orientational diffusion has slowed more than the increase in viscosity would warrant. A change occurs at the mole fraction of 0.2, the same point at which the intermediate power law displays a break and the von Schweidler power law shows an inflection point (see Figure 5). From 0.2 on, the points ascend toward the hydrodynamic line and then increase above it. The rise shows that as the mole fraction (viscosity) continues to be increased, and the orientational diffusion constant does not decrease to the extent that would be dictated by the increasing viscosity. These results demonstrate that the liquid is being modified by the addition of Li^+ in a manner that is more fundamental than a simple increase in viscosity.

The $LiTf_2N$ mole fraction data were also analyzed using MCT for comparison to the temperature-dependent results discussed in Section III.A. The analysis procedure was the same as used above, except that in this case, μ_1 shows a concentration dependence, so it was not fixed at its average value. In both the temperature-dependent and $LiTf_2N$ mole-fraction-dependent data, the translational−rotational coupling constant, κ, increases as the viscosity increases.

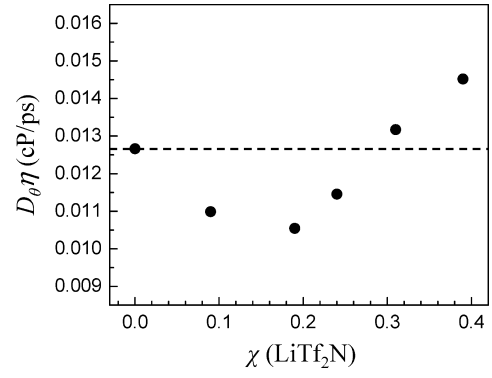

Figure 6. The complete orientation relaxation (α relaxation) diffusion constant multiplied by viscosity plotted versus lithium salt concentration. Hydrodynamic behavior is represented by the dashed line. The nature of the deviation from hydrodynamic behavior changes at the mole fraction $\chi(LiTf_2N) = 0.2$.

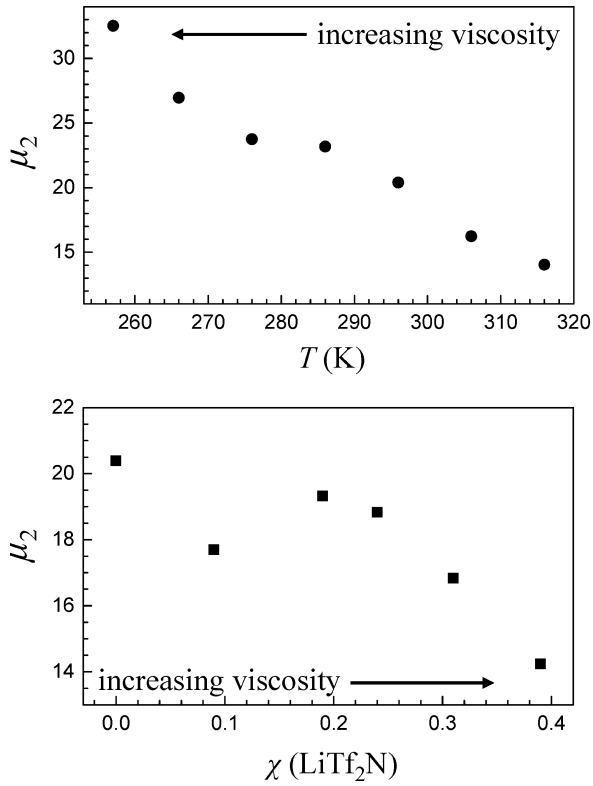

Figure 7. Variation of the schematic MCT damping constant, μ_2, for the orientational relaxation correlation function (eq 7) vs temperature (top panel) and lithium ion concentration (bottom panel). Variation of the temperature and the Li^+ concentration both change the viscosity, but the damping constants show opposite trends.

However, μ_2, the damping constant in the orientational correlation function equation (see eq 7), displays a very different behavior in the concentration and temperature studies. The trends are shown in Figure 7. In the pure liquid (top panel), as the viscosity increases (temperature is lowered), μ_2 increases. In contrast, as the mole fraction of $LiTf_2N$ increases (bottom panel), the viscosity increases, but the orientational oscillator damping constant, μ_2, decreases. Figure 7 also suggests that there is nonmonotonic behavior that occurs at the mole fraction of 0.2. However, in contrast to the data presented above (Figures 5 and 6), it is possible that the anomaly seen in the bottom panel of Figure 7 is a fitting artifact. The results in Figure 7 again show that adding Li^+ to the RTIL has an effect that goes beyond changing the viscosity and reflects, rather, a profound structural change in the liquid that does not occur from changing the temperature. Changes in structure are indicated in MD simulations of similar systems.[13,18]

TABLE 1: Orientational Relaxation Parameters vs. Lithium Cation Concentration

Li^+ mole fraction	viscosity (cP)	τ_α (ps)	D_θ (ps^{-1})
0	59.4	782	2.1×10^{-4}
0.09	74.2	1125	1.5×10^{-4}
0.19	116.1	1836	0.91×10^{-4}
0.24	167.0	2429	0.69×10^{-4}
0.31	294.8	3730	0.45×10^{-4}
0.39	634.6	7283	0.23×10^{-4}

Quitevis and co-workers gave a schematic representation that provides a reasonably good way to visualize the nanostructuring present in the RTIL, although it does not capture the three-dimensional nature of the structures.[52] In Figure 8, we use the same type of representation to indicate the structural changes that may occur in the RTIL systems studied here. The figure shows the differences for three lithium cation concentrations. The qualitative depiction shown in Figure 8 is supported by MD simulations.[13,18] Figure A is for the pure liquid. The figure reflects the nanostructuring that occurs in the pure liquid. On average, in the three-dimension structure, each anion and cation experience the same local environment. Part B has a mole fraction $\chi(LiTf_2N) = 0.2$, which is the mole fraction in Figures 5 and 6, where anomalous behavior is evident. The figure illustrates the proposition that at this concentration, there is sufficient Li^+ concentration to disrupt the nanostructure. The lithium cations have stronger interactions with the anions than the organic cations do. This results in a pairing of anions around Li^+ ions, so the two type of cations in the system are not equivalent in their local environments. In part C, the concentration of Li^+ is higher, with $\chi(LiTf_2N) = 0.4$. Now, Li^+ ions can have larger clusters of anions, three or even four, surrounding them.[18] This clustering moves the structure even further from the pure liquid structure and is also distinct from the structure shown in B. These changes in structure have a major impact on the dynamics of the liquids, as demonstrated by the data presented above (Figures 5−7).

IV. Concluding Remarks

The pure RTIL [bmIm][Tf_2N] was studied using OHD-OKE experiments to measure the liquid's orientational dynamics over the temperatures range 257−316 K. The experiments spanned the time range of ~2 ps to ~10 ns (Figure 1). The data were analyzed in the context of schematic mode coupling theory. The orientational relaxation dynamics (polarizability−polarizability correlation function) consist of two power laws, the intermediate power law and the von Schweidler power law, that are followed by the α relaxation, which is the final exponential complete

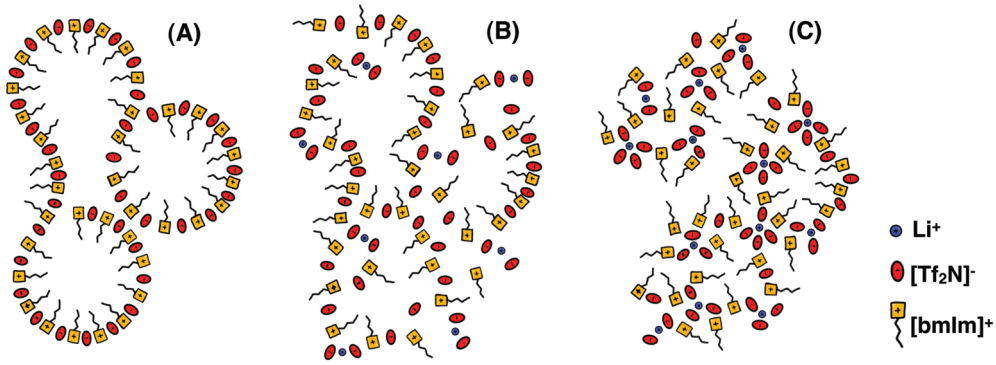

Figure 8. Schematic representations of the RTIL structure with lithium salt concentration. (A) Pure liquid. (B) $\chi(LiTf_2N) = 0.2$. (C) $\chi(LiTf_2N) = 0.4$.

randomization of the molecular orientations. The power law exponents are temperature-independent (Figure 2), but the α relaxation decay time constant is highly temperature-dependent.

The temperature-dependent results obey the MCT scaling relations (Figure 3). In addition, fits to the time-dependent data (Figure 1) using MCT gave the temperature-dependent memory function constants (eq 8). Using the trajectory of these constants and the von Schweidler power law exponent, it was demonstrated that the MCT liquid-to-ideal glass transition could be correctly determined (Figure 4, eqs 10−12). These results show that the dynamical behavior of [bmIm][Tf_2N] is well described in terms of MCT, and they give confidence that we can use parameters associated with MCT in analyzing the influence of lithium ions on [bmIm][Tf_2N].

The OHD-OKE experiments were then used to study the influence of the addition of an inorganic lithium salt to the RTIL to give mixtures [bmIm][Tf_2N] − $LiTf_2N$. The addition of $LiTf_2N$ increases the viscosity of the liquid (see Table 1). Although increasing the salt concentration and decreasing the temperature increases the viscosity of the liquids, the results show that both power law exponents vary with lithium salt concentration (Figure 5), in contrast to the lack of change in their values with changing temperature (Figure 2). The variation of the exponents with lithium salt concentration is not smooth. The intermediate power law exponent z shows a sharp discontinuity at $\chi(LiTf_2N) = 0.2$. The α relaxation was found to display a nonhydrodynamic behavior with increasing lithium salt concentration, which increases the viscosity (Figure 6). The nonhydrodynamic behavior is manifested by a nonconstant value of the product of the orientational relaxation diffusion constant and the viscosity. The nature of the deviation reverses direction at the lithium salt mole fraction of $\chi(LiTf_2N) = 0.2$. The observed breaks in various dynamical observables at $\chi(LiTf_2N) = \sim 0.2$ suggest that the dynamics are influenced by structural changes in the liquid that have been suggested by Raman spectroscopy studies.[14]

Increased Li^+ concentration in RTILs has been associated with decreased Li^+ mobility, which is detrimental to the use of this type of system in battery applications. The results presented here show that there are significant changes in the nature of the liquid's dynamics as the lithium salt concentration is increased, with a break point at $\chi(LiTf_2N) = \sim 0.2$. The experimental results demonstrate that there is a fundamental difference between the viscosity increase caused by the addition of lithium salt and the viscosity increase produced by a decrease in temperature.

Acknowledgment. This work was supported by the Air Force Office of Scientific Research (FA9550-08-1-0306), the National Science Foundation (DMR 0652232), and the Department of Energy (DE-FG03-84ER13251). Additional support was provided by CNPq and FAPESP. We also thank Professor Hans C. Andersen and Dr. Mathias Sperl for useful discussions pertaining to MCT.

References and Notes

(1) Plechkova, N. V.; Seddon, K. R. *Chem. Soc. Rev.* **2007**, *37*, 123.
(2) Armand, M.; Endres, F.; MacFarlane, D. R.; Ohno, H.; Scrosati, B. *Nat. Mater.* **2009**, *8*, 621.
(3) Galinski, M.; Leandowski, A.; Stepniak, I. *Electrochim. Acta* **2006**, *15*, 5567.
(4) Lewandowski, A.; Swiderska-Mocek, A. *J. Power Sources* **2009**, *194*, 601.
(5) Brodd, R. J.; Bullock, K. R.; Leising, R. A.; Middaugh, R. L.; Miller, J. R. *J. Electrochem. Soc.* **2004**, *151*, 1.
(6) Wakihara, M. *Mater. Sci. Eng.* **2001**, *33*, 109.
(7) Kim, K.-S. *Korean J. Chem. Eng.* **2009**, *26*, 770.
(8) Vega, J. A.; Zhou, J.; Kohl, P. A. *J. Electrochem. Soc.* **2009**, *156*, 253.
(9) Ferrari, S.; Quartarone, E.; Mustarelli, P.; Magistris, A.; Protti, S.; Lazzaroni, S.; Fagnoni, M.; Albini, A. *J. Power Sources* **2009**, *194*, 45.
(10) Takada, A.; Imaichi, K.; Kagawa, T.; Takahashi, Y. *J. Phys. Chem. B* **2008**, *112*, 9660.
(11) Rosol, Z. P.; German, N. J.; Gross, S. M. *Green Chem.* **2009**, *11*, 1453.
(12) Umebayashi, Y.; Mitsugi, T.; Fukuda, S.; Fugimori, T.; Fujii, K.; Kanzaki, R.; Takeuchi, M.; Ishiguro, S.-I. *J. Phys. Chem. B* **2007**, *111*, 13028.
(13) Monteiro, M. J.; Bazito, F. F. C.; Siqueira, J. A.; Ribeiro, M. C. C.; Torresi, R. M. *J. Phys. Chem B* **2008**, *37*, 2102.
(14) Duluard, S. J G.; Bruneel, J.-L.; Pianet, I.; Grélard, A.; Campet, G.; Delville, M.-H.; Lassègues, J.-C. *J. Raman Spectrosc.* **2008**, *39*, 123.
(15) Lassègues, J.-C.; Grondin, J.; Christian, A.; Johansson, P. *J. Phys. Chem. A* **2009**, *113*, 305.
(16) Lassègues, J.-C.; Grondin, J.; Talaga, D. *Phys. Chem. Chem. Phys.* **2006**, *8*, 5629.
(17) Hardwick, L. J.; Holzapfel, M.; Wokaun, A.; Novák, P. *J. Raman Spectrosc.* **2007**, *38*, 110.
(18) Borodin, O.; Smith, G. D.; Henderson, W. *J. Phys. Chem. B* **2006**, *110*, 16879.
(19) Ribeiro, M. C. C. *J. Phys. Chem. B* **2003**, *107*, 4392.
(20) Gottke, S. D.; Brace, D. D.; Cang, H.; Bagchi, B.; Fayer, M. D. *J. Chem. Phys.* **2002**, *116*, 360.
(21) Cang, H.; Li, J.; Fayer, M. D. *Chem. Phys. Lett.* **2002**, *366*, 82.
(22) Li, J.; Cang, H.; Andersen, H. C.; Fayer, M. D. *J. Chem. Phys.* **2006**, *124*, 014902.
(23) Li, J.; Wang, I.; Fayer, M. D. *J. Chem. Phys.* **2006**, *124*, 044906.
(24) Hinze, G.; Brace, D. D.; Gottke, S. D.; Fayer, M. D. *J. Chem. Phys.* **2000**, *113*, 3723.
(25) Brace, D.; Gottke, S. D.; Cang, H.; Fayer, M. D. *J. Chem. Phys.* **2002**, *116*, 1598.
(26) Cang, H.; Novikov, V. N.; Fayer, M. D. *Phys. Rev. Lett.* **2003**, *90*, 197401(4).
(27) Smith, N. A.; Meech, S. R. *Int. Rev. Phys. Chem.* **2002**, *21*, 75.
(28) Zhong, Q.; Zhu, X.; Fourkas, J. T. *J. Phys. Chem. B* **2008**, *112*, 3115.
(29) Heisler, I. A.; Meech, S. R. *J. Phys. Chem. B* **2008**, *112*, 12976.
(30) Kamada, K.; Ueda, M.; Sakaguchi, T.; Ohta, K.; Fukumi, T. *Chem. Phys. Lett.* **1996**, *249*, 329.
(31) Zhong, Q.; Fourkas, J. T. *J. Phys. Chem. B* **2008**, *112*, 15529.
(32) Cang, H.; Li, J.; Fayer, M. D. *J. Chem. Phys.* **2003**, *119*, 13017.
(33) Li, J.; Wang, I.; Fruchey, K.; Fayer, M. D. *J. Phys. Chem. A* **2006**, *110*, 10384.
(34) Shirota, H.; Funstonal, A. M.; Wishart, J. F.; Castner, E. W. J. *J. Chem. Phys.* **2005**, *122*, 184512.
(35) Shirota, H.; Castner, E. W. J. *J. Phys. Chem. A* **2005**, *109*, 9388.
(36) Fujisawa, T.; Nishikawa, K.; Shirota, H. *J. Chem. Phys.* **2009**, *131*, 244519.
(37) Götze, W.; Sperl, M. *Phys. Rev. Lett.* **2004**, *92*, 105701.
(38) Cang, H.; Li, J.; Andersen, H. C.; Fayer, M. D. *J. Chem. Phys.* **2005**, *123*, 064508.
(39) McMorrow, D.; Lotshaw, W. T.; Kenney-Wallace, G. A. *IEEE J. Quant. Elec.* **1988**, *24*, 443.
(40) Kai, Y.; Kinoshita, S.; Yamaguchi, M.; Yagi, T. *J. Mol. Liq.* **1995**, *65−6*, 413.
(41) Yan, Y. X.; Nelson, K. A. *J. Chem. Phys.* **1987**, *87*, 6240.
(42) Deeg, F. W.; Stankus, J. J.; Greenfield, S. R.; Newell, V. J.; Fayer, M. D. *J. Chem. Phys.* **1989**, *90*, 6893.
(43) Li, J.; Fruchey, K.; Fayer, M. D. *J. Chem. Phys.* **2006**, *125*, 194501.
(44) Cang, H.; Li, J.; Novikov, V. N.; Fayer, M. D. *J. Chem. Phys.* **2003**, *118*, 9303.
(45) Götze, W. In *Liquids, Freezing and Glass Transition*; Hansen, D. L. J. P., Zinn-Justin, J., Eds.; North-Holland: Amsterdam, 1991.
(46) Bouchaud, J.-P.; Mezard, M. *Prog. Theor. Phys. Suppl.* **1997**, *126*, 181.
(47) Bouchaud, J.-P.; Cugliandolo, L.; Kurchan, J.; Mezard, M. *Physica A* **1996**, *226*, 243.
(48) Götze, W. *Liquids, Freezing and Glass Transition*; Elsevier Science Publishers: Amsterdam, 1989.
(49) Perrin, F. *J. Phys. Radium* **1936**, *7*, 1.
(50) Sension, R. J.; Hochstrasser, R. M. *J. Chem. Phys.* **1993**, *98*, 2490.
(51) Youngren, G. K.; Acrivos, A. *J. Chem. Phys.* **1975**, *63*, 3846.
(52) Xiao, D.; Rajian, J. R.; Hines, L. G. J.; Li, S.; Bartsch, R. A.; Quitevis, E. L. *J. Phys. Chem. B* **2008**, *112*, 13316.

JP103810R